Journal of Power Sources 219 (2012) 272–279

Contents lists available at SciVerse ScienceDirect

Journal of Power Sources

journal homepage: www.elsevier.com/locate/jpowsour

Impacts of anion-exchange-membranes with various ionic exchange capacities on the performance of H_2/O_2 fuel cells

Jie Zhou [a], Junsong Guo [a], Deryn Chu [b], Rongrong Chen [a,*]

[a] Richard G. Lugar Center for Renewable Energy, Indiana University–Purdue University Indianapolis, IN 46202, USA
[b] Army Research Laboratory, Adelphi, MD 20783, USA

HIGHLIGHTS

- Impacts of varying IECs in AEMs on the performance of H_2/O_2 fuel cells were studied.
- The power density of fuel cells using the AEM (0.90 mmol g^{-1}) reached 285 mW cm^{-2} at 50 °C.
- EIS revealed that the OH^- transport resistance was a key factor limiting AEMFC performance.
- The OH^- transport resistance depended on the nature of the AEM and the cell voltages.

ARTICLE INFO

Article history:
Received 14 June 2012
Received in revised form
15 July 2012
Accepted 16 July 2012
Available online 1 August 2012

Keywords:
Anion-exchanged membrane
Block copolymers
Quaternary ammonium
AEM fuel cells
Electrochemical impedance spectra

ABSTRACT

Anion-exchange membranes (AEMs) with varying amounts of quaternary ammonium groups (0.51, 0.70, and 0.90 mmol g^{-1}) grafted onto a styrene–ethylene/butylene–styrene (SEBS) block copolymer were prepared and studied for their impact on the performance of solid electrolyte H_2/O_2 fuel cells. A higher content of quaternary ammonium groups in the membranes resulted in higher ionic conductivity and lower OH^- transport activation energy in the membranes, which in turn resulted in lower cell overpotentials and higher power density in the performance of the AEM fuel cells. By increasing the quaternary ammonium group from 0.51 to 0.90 mmol g^{-1} in the AEMs, the power density of the AEM fuel cells at 50 °C was found to increase from 169 to 285 mW cm^{-2}. For comparison, the performance of AEM fuel cells using a commercial Tokuyamma A901 AEM was also tested. Electrochemical impedance spectra (EIS) recorded during the operation of the AEM fuel cells revealed that the transportation resistance of the OH^- ions from the cathode to the anode through the AEM depended on the nature of the AEM and the cell voltage and is a critical factor to consider for improving the performance of AEM fuel cells.

1. Introduction

Alkaline-based fuel cells as low-cost, high-performance power sources can potentially replace state-of-the-art proton exchange membrane fuel cells (PEMFCs) in many applications [1–10]. Compared with the PEMFCs, the alkaline-based fuel cells have a wider choice of stable and active non-Pt catalysts for oxygen reduction reactions and hydrogen oxidation reactions [11–18]. Using a concentrated alkaline solution, alkaline fuel cells (AFCs) were used as a power source for space shuttle applications, but they continue to face fundamental challenges for applications on the earth because the aqueous KOH electrolyte reacts with the CO_2 from the air to form carbonate species that lower the AFC performance and reduce the lifetime of the cell through the formation of carbonate precipitates on the electrodes [19]. The recently developed alkaline exchange membrane fuel cells (AEMFCs) [20–23] aim to overcome the challenges faced by the AFCs. Since there is no mobile cation in either the AEMs or the electrodes, the formation of carbonate precipitates on the electrodes is no longer a major issue. However, a lack of suitable AEMs and ionomers to meet performance and durability requirements is still one of the major challenges in developing AEMFCs for many applications.

Since 2005, there have been significant efforts to develop AEMs and ionomers by grafting quaternary ammonium groups or quaternary phosphonium groups onto different polymers. The polymers include poly(vinylidene fluoride) (PVDF) [24], poly(tetrafluoroethylene-co-hexafluoropropylene) (FEP) [25], poly(ethylene-co-tetrafluoroethylene), poly(ether imide) [26],

* Corresponding author. Tel.: +1 317 274 4280.
E-mail address: rochen@iupui.edu (R. Chen).

0378-7753/$ – see front matter © 2012 Elsevier B.V. All rights reserved.
http://dx.doi.org/10.1016/j.jpowsour.2012.07.051

poly(arylene ether sulfone) [27], poly(2,6-dimethyl-1,4-phenylene oxide) (PPO) [28], poly(phthalazinone ether ketone) (PPEK) [29], etc. In the last few years, the performance of AEMFCs has been improved significantly, e.g. the peak power capacity has been increased from initially a few mW cm^{-2} to currently 500 mW cm^{-2} [30]. In our previous work [31], we demonstrated that styrene–ethylene/butylene–styrene (SEBS)-based ionomers had excellent dimensional stability and superior performance in AEMFCs due to their unique nanostructures. This work aims to study how varying OH^- conductivity affects the performance of AEMFCs. Three anion exchange membranes were prepared by grafting varying numbers of quaternary ammonium groups onto the SEBS block co-polymer. The ion exchange capacity (IEC), water uptake, swelling, ionic conductivity, and thermal stability of the membranes were tested. Both the performance and the electrochemical impedance spectra (EIS) of AEMFCs with the prepared membranes were studied and compared with those obtained in AEMFCs using the commercial Tokuyamma A901 AEM.

2. Experimental

2.1. Membrane synthesis

Kraton G SEBS A1535 H was purified by precipitation from a 5 wt.% chloroform solution to methanol before chloromethylation. Chloromethylation was carried out following a modified procedure disclosed in our previous work [32]. Specifically, for the chloromethylated SEBS (CMSEBS), 2.5 ml of chloromethyl methyl ether was diluted in 10 ml of chloroform followed by the slow addition of 30 μl of $SnCl_4$ in a three-neck flask equipped with a condenser in an oil bath at 65 °C. After mixing for 30 min, a 5 wt.% SEBS (2 g) chloroform solution was added to the above mixture drop-wise. The solution was stirred for 6–48 h at 65 °C. Chloromethyl functionality was controlled by conversion, which was monitored by ^1H NMR and recorded on a 500 MHz NMR (Bruker Avance II 500 MHz) spectrometer in $CDCl_3$, as shown in Fig. 1. The crude CMSEBS was precipitated in a methanol solution and then washed several times with methanol before being vacuum dried overnight at room temperature. Quarternized SEBS (QSEBS) ionomers were derived from the amination of the CMSEBS with trimethylamine. 2 g of CMSEBS was first dissolved in 40 ml of THF. 10 ml of methanol was then added to the solution to ensure no gelation or precipitation occurred during the quaternization reaction. 2 mol folds of trimethylamine, relative to the chloromethyl group, were slowly added to the solution with adequate agitation. The solution was kept at 40 °C for at least 12 h to guarantee a complete conversion. Membranes (~30 μm thickness) were obtained by casting a quaternized ionomer solution on a PTFE substrate and slowly evaporating the solvents. Then the membranes were heated at 110 °C for 3 h.

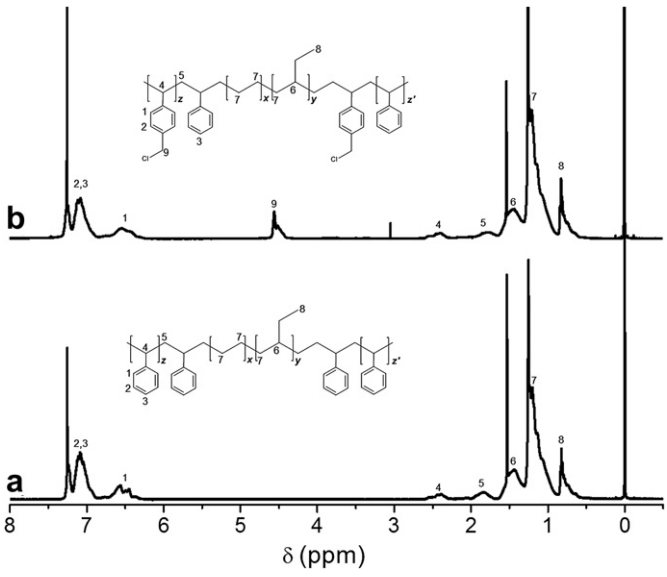

Fig. 1. (a) ^1H NMR spectra of Kraton G SEBS A1535 H and (b) CMSEBS-M in chloroform-*d*.

2.2. NMR characterization

A ^1H NMR (500 MHz) analysis of SEBS for both the starting material and the CMSEBS was performed on a Bruker Avance II 500 MHz instrument using chloroform-*d* as the solvent and tetramethylsilane (TMS) as the internal reference. Since the final ionomers after amination were insoluble in chloroform-*d*, NMR spectra were not acquired.

2.3. Ionic conductivity

Membranes were immersed in 1 M KOH for 48 h to exchange the Cl^- with OH^-. The OH^- ionic conductivity of the membrane was measured using AC impedance spectroscopy with a Solartron 1250 frequency response analyzer interfaced with a Solartron 1287 potentiostat/galvanostat. The measurements were conducted in galvanostatic mode with set frequencies ranging from 0.1 Hz to 60 kHz with the galvanostatically controlled AC current as 5 mA. A standard four-probe conductivity cell (BekkTech LLC, Loveland, CO) was used to assemble the membrane test samples. The tested assembly was completely immersed in de-ionized water pre-equilibrated to the temperature of 30 °C, 40 °C, 50 °C, 60 °C, and 80 °C respectively, and then immediately measured. This was done to eliminate any potential interference caused by reaction of hydroxide ions with dissolved carbon dioxide. Ionic conductivity was calculated as follows:

$$\sigma = \frac{L}{RTW} \tag{1}$$

where L is the length of the membrane between two potential sensing platinum wires in centimeters (cm), R is the membrane resistance in ohms (Ω), T is the thickness of the membrane in cm and W is the width of the membrane in cm.

2.4. Ion-exchange capacity (IEC)

The IEC of the membranes was determined by the back titration method. Approximately 200 mg of membranes (in OH^- form) were immersed in 20 ml of a 0.1 M HCl standard solution for 48 h. The solution was then titrated with a standard solution of potassium hydroxide (0.1 M) to pH 7. After titration, the membrane was soaked in 0.1 M HCl for 48 h then washed and immersed in DI water for 48 h to remove the remaining HCl. It was then vacuum dried at 70 °C for 24 h before being weighed to determine the dry mass (in Cl^- form). The IEC of the membrane was calculated by

$$\mathrm{IEC}\left(\mathrm{mequiv\ g^{-1}}\right) = \frac{M_i - M_f}{m_d} \tag{2}$$

where M_i is the milliequivalents (mequiv) of HCl before membrane neutralization, M_f is the mequiv of HCl measured after neutralization, and m_d is the mass of the dried membrane in grams with Cl^- form.

2.5. Water uptake

The weight differences of membranes before and after soaking in DI water at room temperature for 24 h were used to calculate the water sorption of the membranes. The membranes were weighed immediately after being removed from DI water and after gently blotting the excess water from the surface with tissue paper. Then the membranes were dried overnight at 70 °C by vacuum. The dry membranes were transferred immediately to a desiccator before being cooled to room temperature. The dry membrane weights were recorded and the water sorption of the membranes were calculated by

$$\text{Water Sorption}(\%) = \frac{W_{\text{wet}} - W_{\text{dry}}}{W_{\text{dry}}} \times 100\% \quad (3)$$

where W_{wet} is the weight of the wet membranes in Cl^- forms in grams, and W_{dry} is the weight of the dry membranes in OH^- forms in grams.

2.6. Swelling

Membrane swelling tests were conducted in the same manner as described in our previous study [31]. The membranes in Cl^- form were soaked in a 1.0 M KOH solution for 24 h. The dimension of the wet membrane was measured after quickly wiping the excess water from the surface. Swelling was measured in three directions (x, y, and z directions) by recording the dimensions of the dry membranes and the wet membranes and was calculated using the following equation:

$$\text{Swelling}(\%) = \frac{L_{\text{wet}} - L_{\text{dry}}}{L_{\text{dry}}} \times 100\% \quad (4)$$

where L_{wet} is the length of the wet membranes in cm, and L_{dry} is the length of the dry membranes in cm.

2.7. MEA fabrication

The Tokyamman A4 ionomer was used as the catalyst binder. Catalyst inks for both the anode and cathode consisted of 16 mg of carbon-supported Pt/C (50 wt.% Pt from Alfa Aesar), 2 ml of a THF/methanol mixed solvent, and the A4 ionomer with an 80:20 catalyst to ionomer weight ratio. After homogenizing by sonication, the ink was simply airbrushed onto 6.25 cm^2 of the prepared membranes (~30 μm thick) or the commercial Tokuyamma A901 membranes (~13 μm thick), respectively. The MEA was sandwiched between two pieces of Toray Carbon Paper TGP-H-090 to form a single cell with an active electrode area of 4.5 cm^2. A fuel cell test system (Scribner Associates Model 850e) was used for controlling the cell temperature, humidity, H_2 and O_2 flow rate, and back-pressure. The temperature of the fuel cell was maintained with a tolerance of ±0.2 °C. Fuel cell performance and impedance were tested using an 8-channel Solartron 1470 cell tester. The fuel cells were operated at 50 °C and 20 psi backpressure for both H_2 and O_2 gases. Impedance spectra were recorded by superimposing a 10 mV AC signal on the cell voltages of 0.900, 0.700, 0.500, and 0.300 V in the potentiostatic mode with frequencies ranging from 100 kHz to 0.1 Hz. The electrochemical impedance spectra were simulated by ZSimpWin software.

3. Results and discussion

3.1. Preparation and characterizations of AEMs with varying amounts of functional groups

A commercially available SEBS with styrene composition of 57 wt.% was used as the starting material to prepare membranes with three IECs. The synthetic procedure of the quaternary ammonium SEBS block copolymer for the membrane is shown in Scheme 1. The chloromethylation reaction of the activated aryl ring on the SEBS block co-polymers occurred in a diluted chloroform solution by chloromethyl methyl ether under catalysis of tin(IV) at the reaction temperature of 65 °C. The chloromethylation reaction was monitored by ^{1}H NMR, as shown in Fig. 1. The concentration of attached chloromethyl groups can be controlled by the chloromethylation reaction time from the integrated intensity of peak 9, as shown in Fig. 1b (^{1}H NMR (500 MHz, chloroform-d, 25 °C, TMS): δ=4.5 (s, 2H, CH_2)) to obtain the three final copolymers with different IECs.

Using the back titration method, the IEC of the prepared membranes was tested as 0.51, 0.70, and 0.90 mmol g^{-1}, and the prepared membranes were donated as SEBS:0.51, SEBS:0.70, and SEBS:0.90, respectively. The IEC of the prepared membrane (SEBS:0.90) was very close to the value (0.97 mmol g^{-1}) observed in the commercial Tokuyamma A901 membrane. The relations of ionic conductivity, water uptake, and dimensional stability (swelling) as a function of the IECs of the membranes are shown in Fig. 2 and Table 1. From the results, one can see that the ionic conductivity, water uptake, and swelling of the prepared SEBS membranes and the commercial A901 membrane were proportional to their IEC values. The water uptake and swelling of the prepared SEBS:0.90 membrane with 0.90 mmol g^{-1} IEC were higher than that of the commercial A901 membrane with 0.97 mmol g^{-1} IEC, which indicates that the commercial A901 membrane is dimensionally more stable than our homemade SEBS membranes with a similar IEC value. The conductivity of the membranes is often compromised in order to restrain the swelling. In our earlier work [31], SEBS-based polymeric electrolytes with higher IECs (~1.30 mmol g^{-1}) were successfully prepared and used as ionomer binders for preparing catalyst layers. However, the membranes made from such high IEC polymeric electrolytes were too soft to use for MEAs. As a result, we

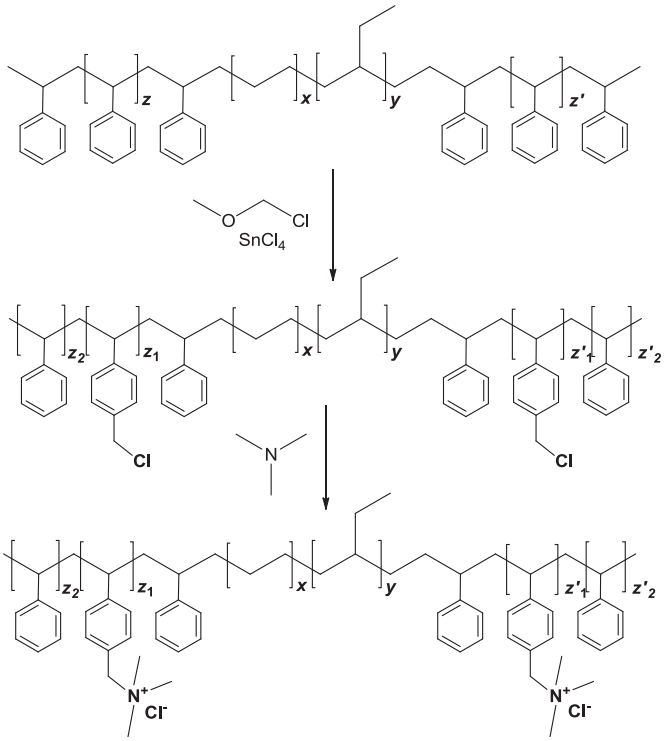

Scheme 1. The synthetic procedure of the quaternary ammonium styrene–ethylene/butylene–styrene block copolymer for membranes in Cl^- form.

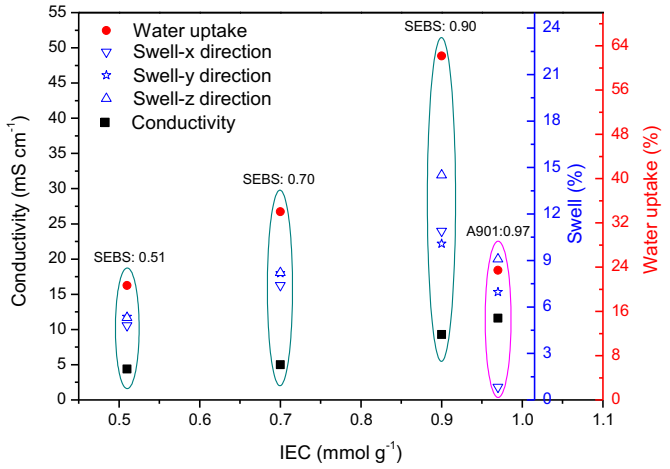

Fig. 2. Ionic conductivity, water uptake, and swelling degree properties as a function of IEC for QSEBS membranes and the Tokuyamma A901 membrane at room temperature.

prepared the tested membranes with moderate IECs. The ionic conductivities of the block copolymer-based SEBS membrane and the commercial A901 membrane as the function of temperatures are shown in Fig. 3a. By increasing the temperature from 30 to 80 °C, all the membranes showed incremental ionic conductivity with the increase in temperature without obvious evidence of conductivity loss for degradation of the functional groups.

Assuming the ionic conductivity of the membranes follows the Arrhenius behavior, the OH^- transportation activation energy E_a in the SEBS:0.51, SEBS:0.70, and SEBS:0.90 membranes can be derived from Fig. 3a and calculated as 20.96, 19.95, and 16.37 kJ mol^{-1}, respectively, by using the equation $E_a = -b^*R$ [25,33], where b is the slope of the regression line of ln σ vs. 1000/T (Fig. 3b), R is the gas constant (8.314 J K^{-1} mol^{-1}), T is the absolute temperature (K), and σ is the OH^- conductivity. Among the three tested SEBS membranes, the membrane (SEBS:0.90) with the highest OH^- conductivity showed the lowest activation energy for the OH^- transportation and had an activation energy (16.37 kJ mol^{-1}) close to that obtained in the Tokuyamma A901 membrane (14.10 kJ mol^{-1}).

3.2. Performance of H_2/O_2 AEMFCs with various AEMs

The performance of the prepared membranes with varying amounts of functional groups grafted onto SEBS copolymers was further studied in AEMFCs. For the comparison, the performance of AEMFCs assembled with Tokuyamma A901 membranes was also tested. The polarization characteristics and power curves obtained in various AEMFCs are presented in Fig. 4a, which shows that varying OH^- conductivity in the membranes had significant impacts on the polarization characteristics and the power capacity of the AEMFCs. Since catalyst layers and gas diffusion layers were identical for both the anodes and cathodes in all the test cells, the observed variations in the polarization and power characteristic

Table 1
IEC, water uptake, swelling degree, and ionic conductivity at room temperature.

IEC (mmol g^{-1})	Water uptake (%)	Swelling degree (x-direction)	Ionic conductivity (mS cm^{-1})
SEBS:0.51	20.67	5.37	4.4
SEBS:0.70	34.00	8.17	5.0
SEBS:0.90	62.15	10.08	9.3
A901:0.97	23.42	6.96	11.6

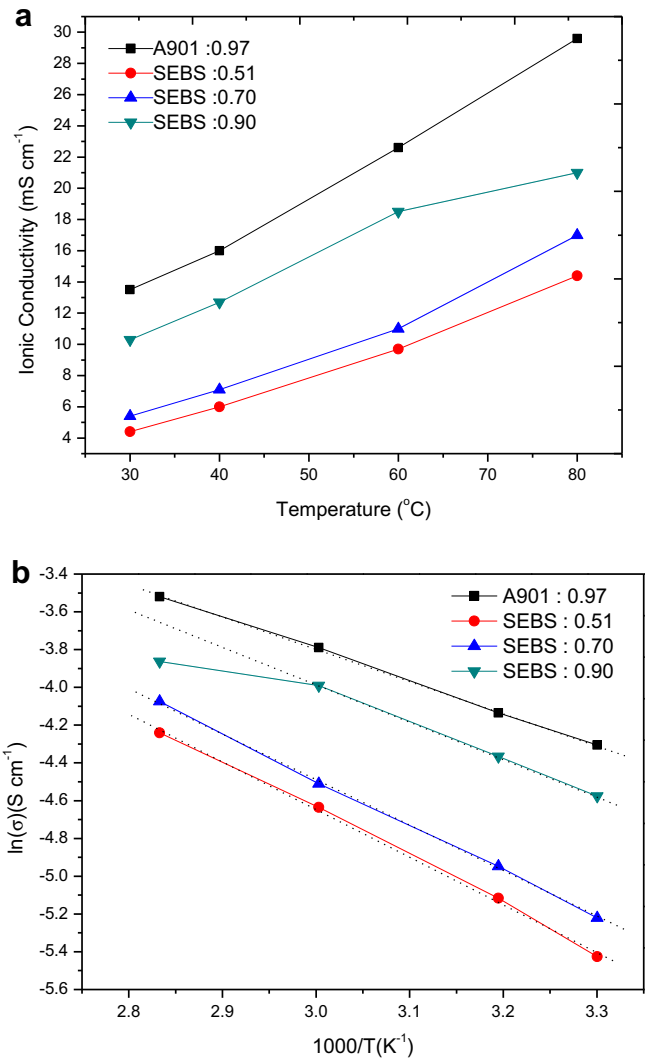

Fig. 3. Ionic conductivity (a) and Arrhenius plots (b) of QSEBS membranes and the Tokuyamma A901 membrane at different temperatures.

curves with various AEMFCs could be mainly caused by the impact of OH^- conductivity in the membranes. The AEMs with higher IECs or higher OH^- conductivity show less polarization and a higher power capacity. The power density of the AEMFCs with AEMs having IEC values of 0.51, 0.70, and 0.90 mmol g^{-1} was 169, 222, and 285 mW cm^{-2}, respectively, at 50 °C, while the power density of the AEM fuel cells with the Tokuyamma A901 membrane was close to 343 mW cm^{-2}. Since the homemade membranes were about 30 μm, which was much thicker than the commercial A901 membrane, IR-corrected polarization curves were also plotted in Fig. 4b. After IR-correction, the AEMFCs using the SEBS membranes with the 0.90 mmol g^{-1} IEC showed the most comparable polarization characteristics to that observed with the Tokuyamma A901 membranes. Although there were various degrees of swelling on the SEBS membranes with different OH^- contents (Fig. 2), the ionic conductivity seems to play a major role in determining the membrane performance in fuel cells: higher OH^- conductivity in the membranes led to less polarizations and higher power capacity. When the polymeric electrolytes were used as the ionomer binders to prepare the catalyst layers, the swelling of the ionomers was found to impact the fuel cell performance much significantly: the ionomers with the higher OH^- conductivity were not guaranteed to have higher performance in AEM fuel cells since the high degree of

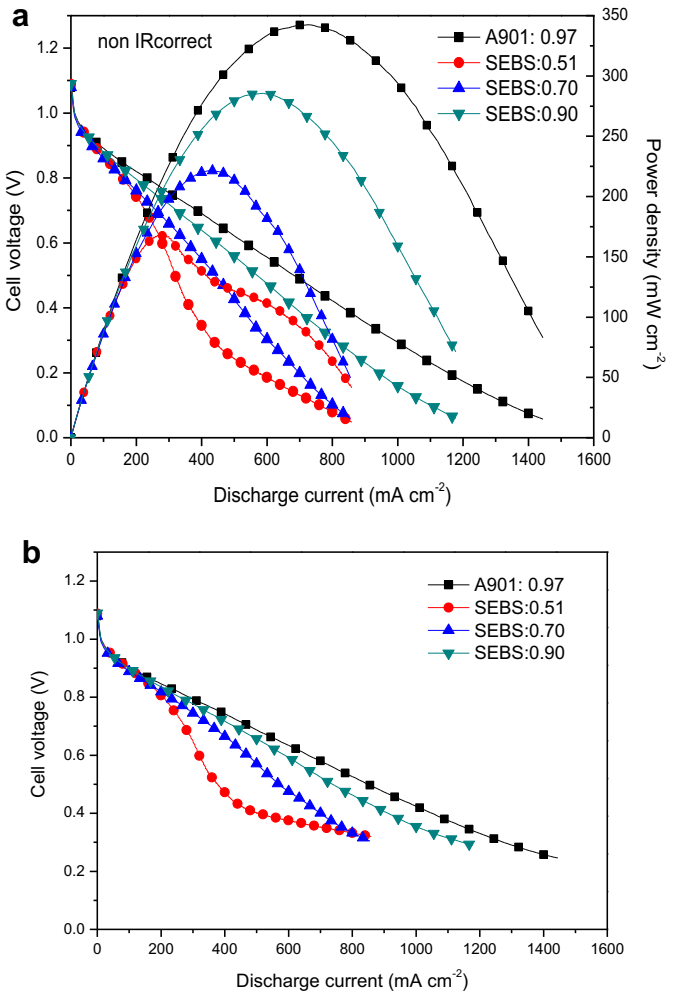

Fig. 4. *I–V* polarization and power density curves of MEAs fabricated with QSEBS membranes and the Tokuyamma A901 membrane. Test conditions: Pt loading = 1 mg cm^{-2} for both the cathode and anode; cell and H_2/O_2 humidifier temperatures=50 °C; H_2 and O_2 flow rates=0.2 L min^{-1} at 20 psi backpressure and 100% RH.

swelling of some of the ionomers resulted extensive cell voltage losses [31].

By carefully examining Fig. 4b, one can see that there were three polarization regions observed on the MEAs with the lowest IEC membranes (SEBS:0.51), in the cell voltage regions of 1.1–0.8 V, 0.8–0.3 V, and 0.3–0.1 V, respectively. These were quite distinct from the polarization curves observed with the other MEAs using higher IEC membranes (SEBS:0.70, SEBS:0.90, and A901), which had two polarization regions. In the low current discharge or high cell voltage region (>0.8 V), the drop in cell voltages as a function of the discharge current density was quite similar for all the test cells with various membranes regardless of the varying OH^- conductivity in the membranes, which indicates that the polarizations in the high cell voltage and low discharge current regions are not significantly affected by the varying OH^- conductivity in the membranes. However, in the cell voltage regions of 0.8–0.3 V, the cell voltages of the MEAs with the SEBS:0.51 membranes dropped the fastest, compared to other MEAs with the same discharge currents. It is revealed that the OH^- conductivity in the membranes had a significant impact on the polarizations of the electrodes in this voltage region: the membranes with lower OH^- conductivity showed higher overpotentials at the same discharge currents. In the low cell voltage (<0.3 V) regions, the MEAs with the membranes having the lowest IEC (SEBS:0.51) showed less voltage drops than those observed in the cell voltage region of 0.8–0.3 V with increasing discharge currents, while the MEAs with the higher IEC membranes (SEBS:0.70 or SEBS:0.90) showed continuing voltage drops with increasing discharge currents. At the cell voltage of 0.1 V, the discharge current densities produced by the MEAs with the SEBS:0.51 membranes became overlapped with those obtained in the MEAs using SEBS:0.70 membranes. In order to better understand the polarization characteristics of MEAs with various membranes at various voltages or currents, electrochemical impedance spectra (EIS) were recorded at various voltages for analyzing how OH^- conductivity in the membranes affects the performance of AEMFCs.

3.3. Electrochemical impedance spectra (EIS) and analysis

The EIS obtained at the cell voltages of 0.900, 0.700, 0.500, and 0.300 V, respectively, are presented in Fig. 5. When the cell voltage was set at 0.900 V, where small discharge currents were obtained in the test cells assembled with various membranes, two impedance loops in the Nyquist plots were obtained (Fig. 5a). According to a previous report [34], the two loops located at the high and low frequency regions can be attributed to the charge transfer impedances of the anode at the high frequency region and the charge transfer impedances for the cathode at the low frequency region. At the cell voltages of 0.700, 0.500, and 0.300 V, as shown in Fig. 5b–d a third loop at the lowest frequency region appeared. The diameter of the third loop was found to depend on not only the OH^- conductivity in the membranes, but also the cell voltages or discharge currents of the AEMFCs. The third loop has been reported by others [34] and referred to the mass transport impedance in a fuel cell. Since we used identical anodes and cathodes in all the AEMFCs in this work, the mass transports of reactants, such as O_2 or water in the cathode and H_2 in the anode, are expected to be similar for all the test cells at the same discharge currents. The largest third loop observed in the EIS with the AEMFCs using the SEBS:0.51 membranes at the cell voltages of 0.700 V and 0.500 V are attributed to the large OH^- transport impedance due to the low OH^- conductivity in the membranes. For the membranes with limited IEC or OH^- conductivity, the OH^- produced at the cathode could not be transported to the anode fast enough and resulted in a local accumulation of OH^- ions on the cathode due to the rather high electrical field presented between the cathode and the anode. When the formed OH^- species were accumulated at the cathode, the positive potentials at the cathode were favorable for the adsorption of OH^- ions on the Pt catalyst surfaces, resulting in losing active sites of Pt catalysts for the oxygen reduction reactions and increasing overpotentials at the cathode or reducing O_2 reduction currents. When the cell voltages dropped to 0.300 V, the diameter of the third loop for the MEAs with the SEBS:0.51 membranes was reduced significantly as compared with those observed at cell voltages of 0.500 and 0.700 V. The diameter of the third loop obtained with the MEAs using either the SEBS:0.70 or SEBS:0.90 membranes increased slightly with increasing discharge currents. Since the membranes with higher IEC or OH^- conductivity could exchange sufficient OH^- ions, the accumulation of OH^- ions at the cathode due to the limited OH^- exchange capacity would not be as significant as that with the SEBS:0.51 membranes. The membranes with higher OH^- conductivities had low overpotentials on their cathodes, resulting in higher discharge currents across a wide voltage region (0.8–0.1 V). At a cell voltage of 0.300 V, the diameter of the third loop observed in the AEMFCs using the SEBS:0.51 membranes was slightly smaller than that in the SEBS:0.70 membranes, mainly due to the different discharge currents obtained at the cell voltage of 0.300 V. The current

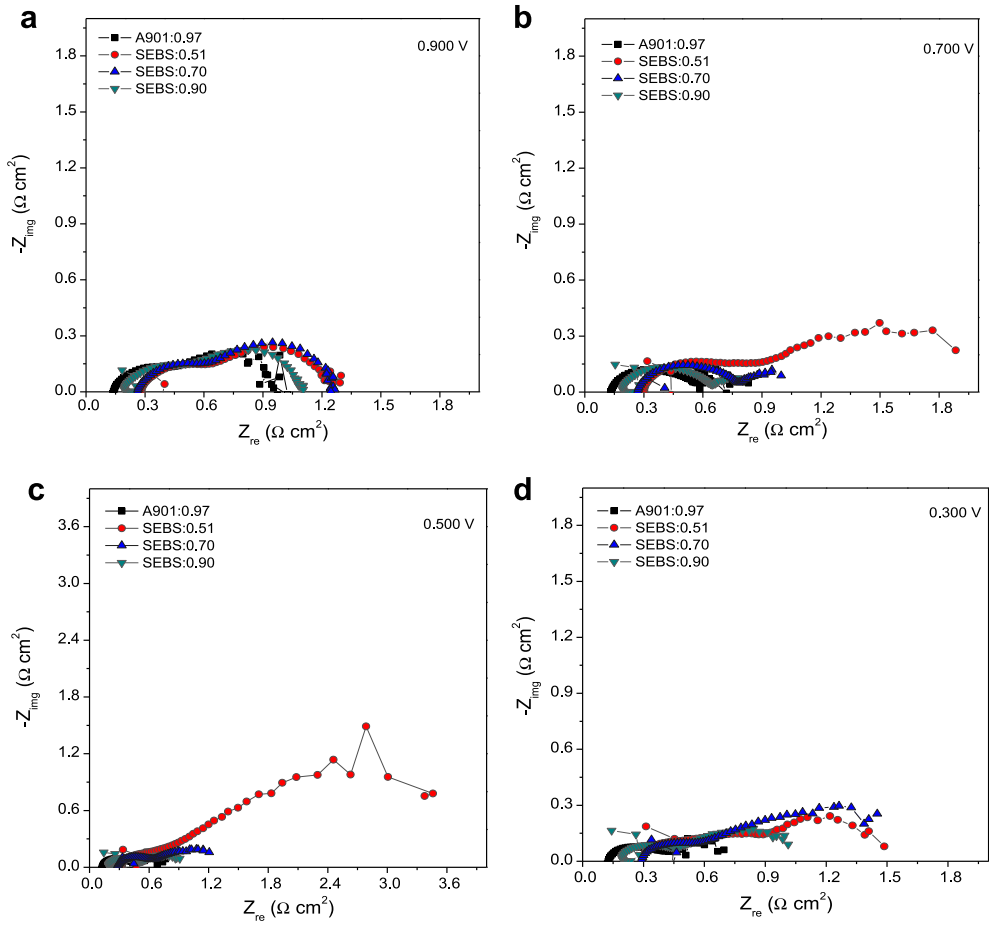

Fig. 5. Electrochemical impedance spectra of the fuel cells with QSEBS membranes and the Tokuyamma A901 membrane at the cell voltage of 0.900 V (a), 0.700 V (b), 0.500 V (c), and 0.300 V (d); 100% RH and 20 psi backpressure for H_2/O_2.

densities recorded at 0.300 V were 410 mA cm^{-2} and 600 mA cm^{-2} for the AEMFCs with SEBS:0.51 and SEBS:0.70 membranes, respectively. A higher current density resulted in higher concentrations of OH^- ions produced at the cathode. If the membrane did not have sufficient OH^- conductivity to transport the large amounts of OH^- produced by the O_2 reduction reactions at high currents, the overpotentials at the cathode increased due to the increased OH^- transport impedance.

Based on the polarization curves of the AEMFCs and the EIS results, it can be seen that (1) the OH^- conductivity in a membrane had a significant impact on the internal impedance and the OH^- transport impedance of the AEMFCs; (2) high cell voltages caused an electric field that was favorable for strong adsorptions of OH^- on the cathode catalysts, resulting in OH^- movement against the concentration gradient and, thus, increased OH^- transport impedance; and (3) discharge current densities affected the OH^- diffusion from the cathode to the anode, and depended on the OH^- exchange capacity in the membranes.

3.4. Models for simulating OH^- transport resistance through AEMs

To better understand the EIS results, the impedance spectra with the high and low frequency loops at the cell voltage of 0.900 V was simulated by using an equivalent circuit shown in Fig. 6a [35,36]. When the OH^- transport limitation (due to the low OH^- conductivity in a membrane) became a significant factor, the third loop appeared in the low frequency region. The EIS was simulated by using the equivalent circuit shown in Fig. 6b [37–41]. Here, R_i is the fuel cell internal resistance, and $R_{a,ct}$ and $R_{c,ct}$ are the charge transfer resistances at the anode and cathode, respectively. The resistance of mass transport at different overpotentials is designated as R_{mass}. Due to the nature of the porous electrodes, the constant phase elements CPE_a, CPE_c, and CPE_{mass} were used in the capacitance simulation.

Table 2 summarizes the simulation results for the EIS obtained at various voltages, as shown in Fig. 5a–d. The values of R_i for the AEM fuel cells with SEBS:0.51, SEBS:0.70, SEBS:0.90, and the commercial A901 membranes were estimated to be 0.28, 0.26, 0.19, and 0.14 Ω cm^2, respectively, which correlates well with the OH^- conductivity of the membranes and points out that the values of R_i were not affected by either the overpotentials or the discharge current densities of the AEMFCs. The charge transfer resistances in both the anode ($R_{a,ct}$) and the cathode ($R_{c,ct}$) were also estimated and are listed in Table 2. Both the values of $R_{a,ct}$ and the $R_{c,ct}$ were not significantly affected by the varying OH^- conductivities in the membranes, but were reduced noticeably by the increasing overpotentials or current densities. The values of $R_{a,ct}$ for various AEMs were estimated to be in the range of 0.28–0.35 Ω cm^2 at a cell voltage of 0.900 V and were reduced to 0.09–0.14 Ω cm^2 at a cell voltage of 0.300 V. Similarly, the values of $R_{c,ct}$ for the various AEMs were in the range of 0.57–0.63 Ω cm^2 at the cell voltage of 0.900 V, and dropped to 0.2 Ω cm^2 at the cell voltage of 0.300 V. The $R_{c,ct}$ was consistently higher than the $R_{a,ct}$ in the entire fuel cell operation voltage region. According to these results, one can see that is essential to reduce the $R_{c,ct}$ and the $R_{a,ct}$, especially at the higher cell voltage regions, to improve the performance of AEMFCs.

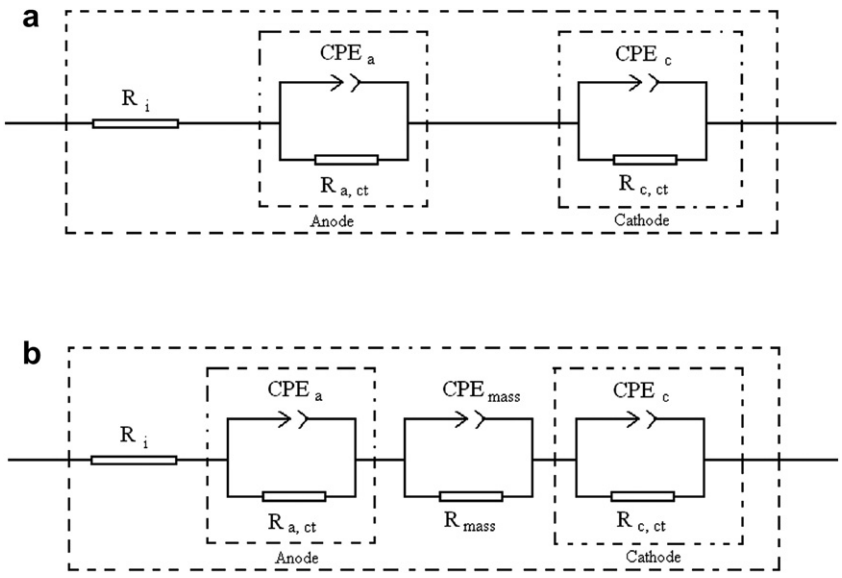

Fig. 6. Equivalent circuits for modeling the electrochemical impedance spectra without (a) and with (b) hydroxide ion transport limitations.

As shown in Table 2, the mass transportation resistance (R_{mass}) appears at 0.700 V and was affected significantly by the OH^- conductivity in the membranes. The membranes with the higher OH^- conductivity showed less R_{mass} at 0.700 V. By increasing the discharge currents or reducing the cell voltages to 0.500 V, the R_{mass} increased more than twice than what was observed at 0.700 V for all the membranes. Again, the membranes with the higher OH^- conductivity showed less R_{mass} at 0.500 V. However, when the cell voltages dropped to 0.300 V, the values of R_{mass} reduced significantly for the Tokuyamma A901 and the SEBS:0.51 membrane. At the cell voltages of 0.700 and 0.500 V, the AEM fuel cells prepared with the SEBS:0.51 membrane showed the highest R_{mass} values, which were 1.156 and 2.911 Ω cm^2, respectively, but were reduced to 0.402 Ω cm^2 at the cell voltage of 0.300 V. The lower R_{mass} with the reduced cell voltages (below 0.300 V) for the SEBS:0.51 membranes resulted in changes in the polarization characteristics in fuel cell performance in this voltage region (Fig. 4b). Since the membranes (SEBS:0.51) with the lowest IEC or OH^- conductivity also had the lowest R_{mass} among the three homemade SEBS-based membranes at the low cell voltage region (<0.3 V), one may wonder if the OH^- conductivity in the membranes was not the controlling factor impacting the R_{mass}. The AEMFCs with both SEBS:0.70 and SEBS:0.90 membranes showed a higher R_{mass} at 0.300 V than those at 0.700 or 0.500 V. The values of the R_{mass} could not be simply correlated to the OH^- conductivity in the membranes, which likely also includes other resistances from the mass transport of O_2, H_2, or H_2O.

As we know, an electric field is present between the cathode and the anode in a membrane (10–30 μm). When an AEM fuel cell is operating at a high cell voltage region (>0.8 V), the potential of the cathodes is much positive than the potential of the anode. Because a positive electric field is favorable for the adsorption of OH^- on the Pt cathode catalyst, a fraction of the electrochemically active sites on the Pt/C catalysts can be blocked and result in increasing charge transfer impedances of the $R_{c,ct}$ and $R_{a,ct}$. By reducing the cell voltages, the electric field responsible for the OH^- drag at the cathode was weakened and resulted in not only reducing the charge transfer resistances, but also reducing the R_{mass} at the same discharge currents since the OH^- diffusion is mainly governed by the concentration gradient of the OH^-, and the OH^- exchange capacity

Table 2
Key parameters derived from the EIS (Fig. 5) by using the equivalent circuit (Fig. 6).

Sample	Cell voltage	$R_{a,ct}$ (Ω cm^2)	CPE_a, Q (F cm^{-2})	CPE_a, n	R_i (Ω cm^2)	$R_{c,ct}$ (Ω cm^2)	CPE_c, Q (F cm^{-2})	CPE_c, n	R_{mass} (Ω cm^2)	CPE_{mass}, Q (F cm^{-2})	CPE_{mass}, n
A901:0.97	0.900	0.2835	0.004549	0.8264	0.1412	0.5884	0.08689	0.7542	–	–	–
	0.700	0.1607	0.001561	0.9538	0.1381	0.2671	0.03026	0.7527	0.2465	1.899	0.8634
	0.500	0.1209	0.0009128	1	0.1366	0.1698	0.0179	0.8314	0.458	1.27	0.6375
	0.300	0.09532	0.001106	1	0.1319	0.1882	0.04219	0.7121	0.2962	1.486	0.713
SEBS:0.51	0.900	0.3709	0.006926	0.7599	0.2765	0.6011	0.07873	0.8124	–	–	–
	0.700	0.2421	0.002178	0.8804	0.2987	0.3491	0.04028	0.7029	1.156	0.5327	0.6616
	0.500	0.2014	0.002622	0.8604	0.3117	0.6865	0.09623	0.5634	2.911	0.2311	0.7564
	0.300	0.1399	0.001392	0.9307	0.2856	0.6035	0.1064	0.549	0.4021	1.068	1
SEBS:0.70	0.900	0.3713	0.006731	0.7735	0.2596	0.6381	0.07024	0.8379	–	–	–
	0.700	0.1729	0.001931	0.924	0.2707	0.3274	0.02229	0.7546	0.3707	3.099	0.6593
	0.500	0.1206	0.0007918	1	0.2862	0.1735	0.01119	0.8542	0.9021	0.7689	0.5073
	0.300	0.1039	0.000784	1	0.2936	0.1978	0.006266	0.7801	1.676	0.5477	0.4146
SEBS:0.90	0.900	0.3469	0.006975	0.7651	0.1899	0.5691	0.06935	0.8112	–	–	–
	0.700	0.1337	0.001768	0.935	0.1902	0.3132	0.01598	0.7628	0.228	2.958	0.7179
	0.500	0.1113	0.0007106	1	0.1945	0.1725	0.007786	0.8724	0.519	0.8054	0.5834
	0.300	0.09527	0.000686	1	0.1927	0.1208	0.00686	0.9078	0.7758	0.5748	0.514

of the membranes. As shown in Fig. 4b, fewer drops in cell voltage were observed on the AEMFCs with the higher IEC membranes at the same current densities. For the AEMFCs with the lowest IEC membranes (SEBS:0.51), significant cell voltage drops in the voltage region of 0.8–0.3 V (Fig. 4b) could have contributed to the low OH^- exchange capacity in the membranes, which caused the accumulation of OH^- at the cathode and increased the $R_{c,ct}$, R_{mass}, and $R_{a,ct}$. However, the limitation of OH^- transport can be mitigated by reducing the electrical field at the lower cell voltage (<0.3 V). The SEBS:0.51 membrane showed an improved performance at a low cell voltage (<0.3 V). This finding is very important to understand the OH^- transport mechanism in anion exchange membranes. Increasing the amounts of functional groups or IECs in polymeric electrolytes can improve the OH^- transport routes, which can lessen the impacts by the electric field for OH^- drag at the cathode in high cell voltage regions, as demonstrated by the improved AEMFC performance observed in the high functional group membranes, such as the SEBS:0.90 and the Tokuyamma A901 membranes.

4. Conclusion

In this study, anion-exchange membranes with varying amounts of quaternary functional groups on a styrene–ethylene/butylene–styrene (SEBS) block copolymer were successfully developed for solid H_2/O_2 fuel cells. With the prerequisite of a high mechanical strength for the preparation of the membrane of electrode assemblies, the ionic conductivity of the membranes was able to be improved by increasing the amount of quaternary functional groups on the SEBS polymers. From the polarization curves and the electrochemical impedance spectra of fuel cells with varying functionalized membranes, it was revealed that an electric field was present between the anode and the cathode against the OH^- transportation from the cathode to the anode, especially at the higher cell voltage regions. When the OH^- transport channels were limited in the membranes that contained fewer functional groups, or when the intensity of the electric field was very strong at the high cell voltage regions, the OH^- transport resistance became a controlling factor to cause severe polarizations in the fuel cells. It was demonstrated that increasing the OH^- conductivity in a membrane reduced internal impedance, reduced OH^- transport impedance, and reduced OH^- dragging effects at the cathode due to the strong electric field, which also led to a significant reduction in the electrode overpotentials during the operation of the AEM fuel cell.

Acknowledgments

This work was sponsored by the Army Research Laboratory (Grant no. W911NF-10-2-0075). The Kraton G SEBS A1535 H sample was kindly provided by Kraton Performance Polymers, Inc.

References

[1] E.D. Geeter, M. Mangan, S. Spaepen, W. Stinissen, G. Vennekens, J. Power Sources 80 (1999) 207–212.
[2] K. Kordesch, J. Gsellmann, M. Cifrain, S. Voss, V. Hacker, R.R. Aronson, C. Fabjan, T. Hejze, J. Daniel-Ivad, J. Power Sources 80 (1999) 190–197.
[3] B.Y.S. Lin, D.W. Kirk, S.J. Thorpe, J. Power Sources 161 (2006) 474–483.
[4] A. Verma, S. Basu, J. Power Sources 145 (2005) 282–285.
[5] A.M. Bartrom, J.L. Haan, J. Power Sources 214 (2012) 68–74.
[6] Z.X. Liang, T.S. Zhao, J.B. Xu, L.D. Zhu, Electrochim. Acta 54 (2009) 2203–2208.
[7] A. Serov, C. Kwak, Appl. Catal., B: Environ. 98 (2010) 1–9.
[8] D. Wang, J. Liu, Z. Wu, J. Zhang, Y. .Su, Z. Liu, C. Xu, Int. J. Electrochem. Sci. 4 (2009) 1672–1678.
[9] L. Demarconnay, S. Brimaud, C. Coutanceau, J.M. Leger, J. Electroanal. Chem. 601 (2007) 169–180.
[10] K. Matsuoka, Y. Iriyama, T. Abe, M. Matsuoka, Z. Ogumi, J. Power Sources 150 (2005) 27–31.
[11] X. Wu, K. Scott, J. Power Sources 206 (2012) 14–19.
[12] Z. Liu, Z. Li, H. Qin, B. Liu, J. Power Sources 196 (2011) 4972–4979.
[13] H. Qin, Z. Liu, S. Lao, J. Zhu, Z. Li, J. Power Sources 195 (2010) 3124–3129.
[14] G. Ma, R. Jia, J. Zhao, Z. Wang, C. Song, S. .Jia, Z. Zhu, J. Phys. Chem. C 115 (2011) 25148–25154.
[15] C. Rao, Y. Ishikawa, J. Phys. Chem. C 116 (2012) 4340–4346.
[16] Z. Yang, X. Zhou, H. Nie, Z. Yao, S. Huang, Appl. Mater. Interfaces 3 (2011) 2601–2606.
[17] W. Sun, A. Hsu, R. Chen, J. Power Sources 196 (2011) 627–635.
[18] J. Guo, H. Li, H. He, D. Chu, R. Chen, J. Phys. Chem. C 115 (2011) 8494–8502.
[19] J.R. Varcoe, R.C.T. Slade, Fuel Cells 5 (2005) 187–200.
[20] K. Matsumoto, T. Fujigaya, H. Yanagi, N. Nakashima, Adv. Funct. Mater. 21 (2011) 1089–1094.
[21] M. .Unlu, J. Zhou, P.A. Kohl, Electrochem. Solid-State Lett. 12 (2009) B27–B30.
[22] S. Gu, R. Cai, T. Luo, Z. Chen, M. Sun, Y. Liu, G. He, Y. Yan, Angew. Chem., Int. Ed. 48 (2009) 1–5.
[23] J. Pan, S. Lu, Y. Li, A. Huang, L. Zhuang, J. Lu, Adv. Funct. Mater. 20 (2010) 312–319.
[24] T.N. Danks, R.C.T. Slade, J.R. Varcoe, J. Mater. Chem. 12 (2002) 3371–3373.
[25] R.C.T. Slade, J.R. Varcoe, Solid State Ionics 176 (2005) 585–597.
[26] G. Wang, Y. Weng, D. Chu, D. Xie, R. Chen, J. Membr. Sci. 326 (2009) 4–8.
[27] G. Wang, Y. Weng, D. Chu, R. Chen, D. Xie, J. Membr. Sci. 332 (2009) 63–68.
[28] Y. Li, T. Xu, J. Appl. Polym. Sci. 114 (2009) 3016–3025.
[29] H. Zhang, Z. Zhou, J. Appl. Polym. Sci. 110 (2008) 1756–1762.
[30] M. Mamlouk, K. Scott, J. Power Sources 211 (2012) 140–146.
[31] L. Sun, J. Guo, J. Zhou, Q. Xu, D. Chu, R. Chen, J. Power Sources (2012) 70–77.
[32] G. Wang, Y. Weng, J. Zhao, D. Chu, D. Xie, R. Chen, Polym. Adv. Technol. 21 (2010) 554–560.
[33] Q.H. Zeng, Q. Li Liu, I. Broadwell, A.M. Zhu, Y. Xiong, X.P. Tu, J. Membr. Sci. 349 (2010) 237–243.
[34] W.H. Zhu, R.U. Payne, B.J. Tatarchuk, J. Power Sources 168 (2007) 211–217.
[35] J. Zhang, Y. Tang, C. Song, J. Zhang, H. Wang, J. Power Sources 163 (2006) 532–537.
[36] J. Zhang, Y. Tang, C. Song, X. Cheng, J. Zhang, H. Wang, Electrochim. Acta 52 (2007) 5095–5101.
[37] M. Ciureanu, R. Roberge, J. Phys. Chem. B 105 (2001) 3531–3539.
[38] A. Arvay, E. Yli-Rantala, C.H. Liu, X.H. Peng, P. Koski, L. Cindrella, P. Kauranen, P.M. Wilde, A.M. Kannan, J. Power Sources 213 (2012) 317–337.
[39] X. Yuan, J.C. Sun, M. Blanco, H. Wang, J. Zhang, D.P. Wilkinson, J. Power Sources 161 (2006) 920–928.
[40] S. Asghari, A. Mokmeli, M. Samavati, Int. J. Hydrogen Energy 35 (2010) 9283–9290.
[41] Y. Tang, J. Zhang, C. Song, H. Liu, J. Zhang, H. Wang, S. Mackinnon, T. Peckham, J. Li, S. McDermid, P. Kozak, J. Electrochem. Soc. 153 (2006) A2036–A2043.